Journal Pre-proofs

Stochastic Fatigue Damage in Viscoelastic Materials using Probabilistic Pseudo J-Integral Paris' Law

Hui Li, Xue Luo, Yuqing Zhang, Rongqiao Xu

Please cite this article as: Li, H., Luo, X., Zhang, Y., Xu, R., Stochastic Fatigue Damage in Viscoelastic Materials using Probabilistic Pseudo J-Integral Paris' Law, *Engineering Fracture Mechanics* (2021), doi: https://doi.org/10.1016/j.engfracmech.2021.107566

Stochastic Fatigue Damage in Viscoelastic Materials using Probabilistic Pseudo J-Integral Paris' Law

Hui Li

College of Civil Engineering and Architecture

Zhejiang University

866 Yuhangtang Road, An-zhong Bldg.

Hangzhou 310058, Zhejiang, China

Email: huili94@zju.edu.cn

Xue Luo

(corresponding author)

College of Civil Engineering and Architecture

Zhejiang University

866 Yuhangtang Road

Hangzhou 310058, Zhejiang, China

Yuqing Zhang

Aston Institute of Materials Research

Aston University

Aston Triangle, Birmingham, B4 7ET, U.K.

Phone: +44 (0) 121-204-3391

Email: y.zhang10@aston.ac.uk

Rongqiao Xu

College of Civil Engineering and Architecture

Zhejiang University

866 Yuhangtang Road, An-zhong Bldg.

Hangzhou 310058, Zhejiang, China

Email: xurongqiao@zju.edu.cn

Damage density of viscoelastic materials is derived based on an energy-based mechanistic approach.

Damage evolution rate of viscoelastic materials is established by pseudo J-integral Paris' law.

A stochastic fatigue damage model is proposed to track entire damage process of viscoelastic materials.

Abstract

Fatigue damage of engineering materials severely affects the serviceability of their structures. It is impracticable to accurately predict fatigue damage process of engineering materials due to the variability of material properties, microstructure heterogeneity and others. This study aims to track the entire fatigue damage process by coupling the variability into a fatigue damage mechanism for engineering materials. A typical viscoelastic material, asphalt binder, widely used in pavement engineering is selected for investigation in this study. The pseudo J-integral Paris' law model and probability theory are combined to establish a stochastic fatigue damage model for viscoelastic asphalt materials. Results show that the damage density can be determined by an apparent shear modulus and true shear modulus. The damage evolution rate is a function of material parameters (Paris' law coefficients), apparent shear modulus, apparent shear strain amplitude and apparent phase angle. Then, a cumulative distribution function of loading time (TCDF) and damage density exceedance probability (DDEP) are derived and experimentally verified. Next, a stochastic fatigue damage model is proposed, which can track the entire fatigue damage process for viscoelastic materials, and it depends on the damage density, material parameters and variability parameters. The variability of minor damage can be used to predict the variability of severe damage based on the stochastic fatigue damage model.

Keywords: Stochastic fatigue damage; viscoelastic materials; pseudo J-integral Paris' law; probability.

1 Introduction

Fatigue damage of many engineering materials (such as asphalt materials in road engineering, aluminum alloy materials in aerospace and so on) is generally caused by cyclic loading. It makes the serviceability of their structures deteriorate with time. A representative viscoelastic material, asphalt binder, widely used in road engineering is selected for investigation in this study. Fatigue damage of asphalt pavements is closely related to the cohesive failure within the asphalt binder. It is of great significance to characterize and understand the fatigue behavior of the asphalt binder for evaluating the service life of asphalt pavements. Therefore, some indicators and fatigue damage models have been proposed to characterize the fatigue behavior for the asphalt binder, which can be generally classified as: (1) empirical indicators; (2) dissipated energy indicators; and (3) mechanical fatigue damage models.

Many empirical and dissipated energy indicators were proposed to characterize the fatigue failure for the asphalt binder. On one hand, some empirical indicators were utilized as fatigue failure criterion, such as a 50% loss of stiffness [1] and pseudo-stiffness [2], a peak of phase angle [3]. Besides, a fatigue factor $|G^*|\cdot sin\delta$ ($|G^*|$ is shear modulus and δ is phase angle) was established to quantify the fatigue resistance of asphalt binders [4]. On the other hand, several dissipated energy indicators were proposed to reflect the fatigue behavior of asphalt binders based on mechanical principles and material properties, which contain a dissipated energy ratio (DER) [5], [6], [7] and the ratio of dissipated energy change (RDEC) [8], [9], [10].

From the perspective of mechanical fatigue damage models, the entire fatigue damage process of the asphalt binder was studied. Hintz and Bahia [11], Shan et al. [12]

proposed the crack length model for asphalt binders to characterize the entire fatigue damage process under a rotational shear fatigue load. However, it is imprecise to use a linear viscoelastic constitutive equation at undamaged state to derive crack length at damage stage. Hence, a damage mechanics-based crack length model has been formulated to analyze the fatigue cracking for asphalt binders [13] [14].

These indicators and fatigue damage models promote understanding of the fatigue damage process of asphalt binders. However, all the indicators and fatigue damage models aforementioned are deterministic. In other words, the mean values of test results are taken to quantify the fatigue behavior of the materials. As a matter of fact, the variability associated with material properties, microstructure heterogeneity and others cause the uncertainty of fatigue damage process for many engineering materials [15], [16], [17], [18]. If these deterministic fatigue indicators and fatigue damage models are applied in structures made up of such materials, the estimation bias will lead to unintended consequences. Therefore, some probabilistic fatigue damage models have been proposed to characterize the scatter of the fatigue damage data for some engineering materials, which contain phenomenological probabilistic fatigue damage model and mechanical probabilistic fatigue damage model.

In the phenomenological probabilistic damage models, the mean value and standard deviation are predicted by fitting crack growth test data [19]. In addition, Kozin and Bogdanof [20], [21] established a B-model based on the mathematical concept of Markov chains, which can obtain the stochastic characteristics of fatigue cracking damage in the service life. It has become a popular method for solving probabilistic fatigue cracking damage problems due to the simplicity of the model. However, fatigue damage mechanisms are neglected in these phenomenological probabilistic damage models.

To overcome this limitations, some mechanics-based probabilistic fatigue damage models were proposed based on fatigue damage mechanism of the materials. A representative model was Yang and Manning's stochastic fatigue crack growth model

[22]. The model was established by adding a random variable into the Paris' law equation which can characterize the fatigue damage mechanism. Some researchers focused on studying the statistical variability of damage evolution by this model [23], [24], [25], [26].

However, these mechanical fatigue damage models only apply to non-viscous materials. For the viscoelastic materials, large-scale yielding of fatigue crack growth occurs when performing a fatigue load to materials. Hence, Yang and Manning's stochastic fatigue crack growth model related to the stress intensity factor is limited. A probabilistic viscoelastic continuum damage model was employed to analyze the variability of asphalt materials [27], [28], [29]. Nevertheless, only the probability distribution curve of fatigue life was analyzed, and stochastic damage analysis for the entire fatigue damage process was not implemented and tracked.

As a result, coupling the variability into fatigue damage mechanism to track the entire fatigue damage process for viscoelastic materials is of more practical significance. To better overcome the limitation above-mentioned, it is necessary to fundamentally investigate the stochastic fatigue damage process of viscoelastic materials. Hence, the objective of this work is to develop a stochastic fatigue damage model which can track the entire fatigue damage process of viscoelastic materials based on a mechanistic method and probability theory. Typical asphalt binders are tested and analyzed to illustrate the method as well as the results.

This study is organized as follows. First, materials and laboratory tests are elaborated. Second, a shear stress and shear stress model are established and an energy-based mechanistic (EBM) approach is utilized to derive a deterministic fatigue damage model for the asphalt binder. Besides, the variability of fatigue damage evolution of the asphalt binders is analyzed. Then, a random variable is added into the deterministic fatigue damage model to randomize the model and model parameters are estimated based on a maximum likelihood estimation approach. Next, a cumulative distribution function of loading time (TCDF) and damage density exceedance probability (DDEP)

are calculated and verified. In addition, a stochastic damage model coupled variability into fatigue damage mechanism is determined for the asphalt binder. Finally, a summary section concludes this study with the main results.

2 Materials and Laboratory Tests

2.1 Materials

A typical viscoelastic material, asphalt binder commonly used in road engineering, was selected in this study. Basic indicators (penetration, softening point and ductility) of the asphalt binder were tested by specification methods [30]. These test results of all the basic indicators and properties are shown in the Table 1. It indicates that the basic indicators and properties meet the technical requirement in the specification [30].

Materials	Properties	Units	Requirements	Results
Asphalt binder	Penetration at 25℃	0.1mm	40-60	56
	Softening point	℃	≥60	88.4
	Ductility at 15℃	cm	≥20	36.5

Table 1. Basic indicators and properties of the asphalt binder

2.2. Equipment and Sample Preparation

The Discovery Hybrid Rheometer (DHR) from TA Instruments was used to perform tests for asphalt binders in this study. An 8-mm diameter parallel plate was employed. Therefore, the size of the asphalt binder sample was 8mm in diameter. An equipment and sample preparation of the test are shown in Fig. 1. The sample preparation consists of the following steps:

(1) Make asphalt binder samples: heat the asphalt binders in the oven until it flows, and pour the hot asphalt binders into the silicon rubber mould. Then, cooling it to the room temperature. An asphalt binder sample is shown in Fig. 1.

(2) Place the asphalt binder sample in the instrument: the sample was removed by bending the rubber mould and adhered it to the lower parallel plate of the instrument by gently pressing the top surface of the sample. This step was to avoid adhesive failure between the asphalt binder and the parallel plate during the test.

(3) Set test parameters: set up a trim gap (2050μm), target gap (2000μm), test type, temperature and loading time, etc. It's worth mentioning that the extra 50μm between the trim gap and target gap can ensure that a proper lateral bulge is formed at the outside edge of the asphalt binder sample in the next step.

(4) Trim the asphalt binder sample: press a trim button of the instrument, the gap between upper parallel plate and lower parallel plate would go to the trim gap. Then, rock the rotating lever, and a heated trimming tool was used to trim the extra asphalt binder. It makes the outside diameter of the asphalt binder sample equal the outer diameter of the plates. The trim gap is presented in Fig. 1.

(5) Complete the sample preparation: when the trimming process was finished, the upper parallel plate was lowered to the target gap as shown in Fig. 1. In addition, to avoid uneven temperature distribution throughout the entire asphalt binder sample, the sample was heated to the target testing temperature and kept for 5 min. At this point, the preparation of the sample was completed.
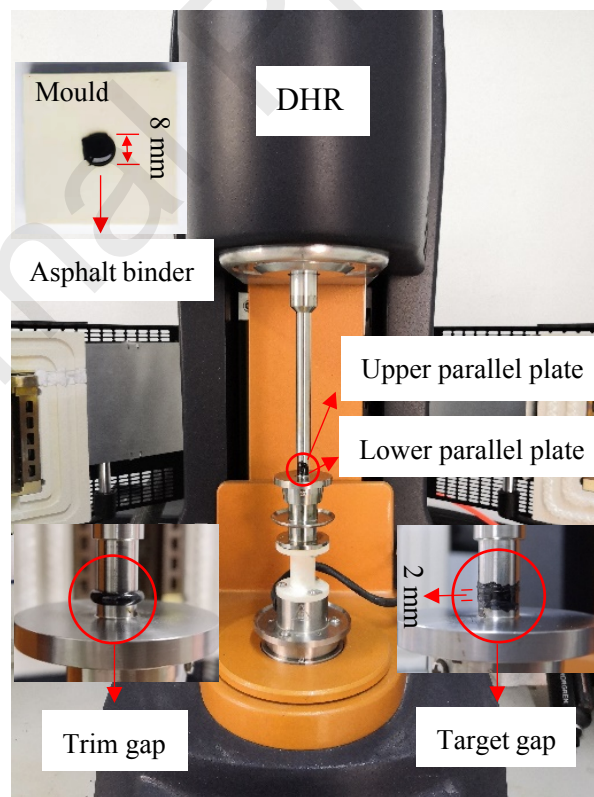
Fig. 1. Equipment and sample preparation of the test

2.3 Test Methods

When the sample preparation was completed, time sweep tests were performed. Applying a sinusoidal loading to the asphalt binder sample, the maximum shear strain amplitude was formed at the edge of cylindrical specimen. Thirty repetitive time sweep tests are performed for the asphalt binders. All of time sweep tests were conducted at 4% of oscillation shear strain amplitude, at the temperature of 25°C and the loading frequency of 10 Hz. Shear moduli and phase angles cab be obtained in time sweep tests, which are particularly important to characterize the fatigue damage evolution of the asphalt binder. Fig. 2 shows typical relationship between the shear moduli/phase angles of the asphalt binder and loading time at 4%, 25°C and 10 Hz. It is found that the shear modulus decreases with the loading time. The phase angle increases to the peak and then decreases with the loading time, and it fluctuates at the later loading stage. These observation results of the shear modulus and phase angle are caused by fatigue damage process of the asphalt binder sample.
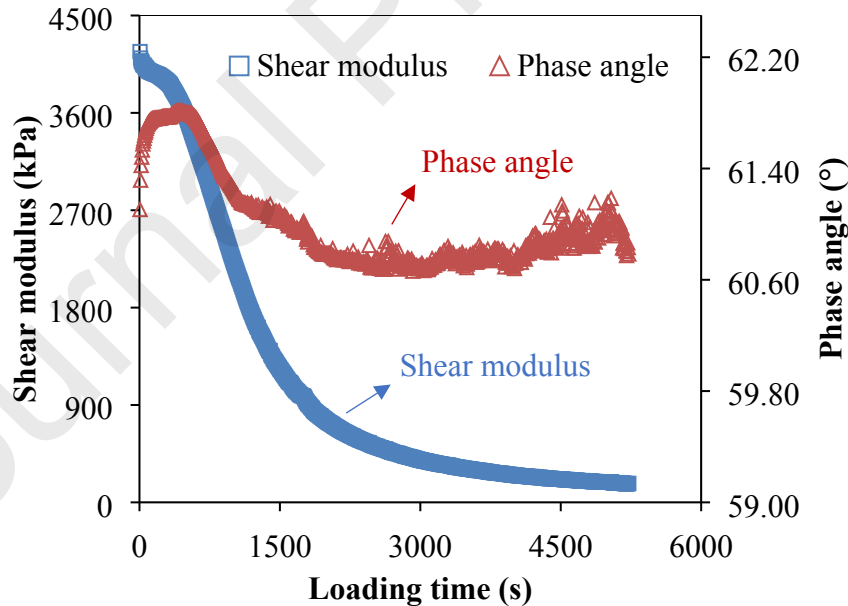
Fig. 2. Typical relationship between the shear moduli/phase angles of the asphalt binder and loading time of 4%, 25°C and 10 Hz

3. Establishment of Deterministic Fatigue Damage Model for Asphalt Binders

To obtain the stochastic fatigue damage model reflecting the fatigue damage

mechanism and variability of asphalt binders, the deterministic fatigue damage model should be established first. This section contains the following three aspects:

(1) Formulate the shear strain and shear stress models for asphalt binders;

(2) Establish the deterministic fatigue damage model for asphalt binders; and

(3) Analyze the variability for fatigue damage results calculated by the deterministic fatigue damage model.

3.1 Formulation of Shear Strain and Shear Stress Model for Asphalt Binders

When performing the time sweep test, edge cracks of a cylindrical asphalt binder specimen will generate and gradually expand to the loading center with the loading time. For the cylindrical asphalt binder sample in the test, the intact material (exclude the invalid volume caused by crack growth) is called intact asphalt binder, and the entire material including cracks is called apparent asphalt binder. The shear strain, shear stress, torque and energy dissipation of the intact asphalt binder are certainly different from those in the apparent asphalt binder. In this study, these mechanical variables in the intact asphalt binder are called "true shear stress", "true shear strain", "true torque" and "true energy". Correspondingly, those in the apparent asphalt binder are defined as the "apparent shear strain", "apparent shear strain", "apparent torque" and "apparent energy", respectively.

First, the shear strain and shear stress of the apparent asphalt binder and the intact asphalt binder are formulated. Fig. 3 presents distribution of shear strain/shear stress in the intact asphalt binder and the apparent asphalt binder. It is worth mentioning that the shear stress and shear strain are constant function in z direction, θ direction and increase linearly in r direction when performing a strain-controlled rotational load.
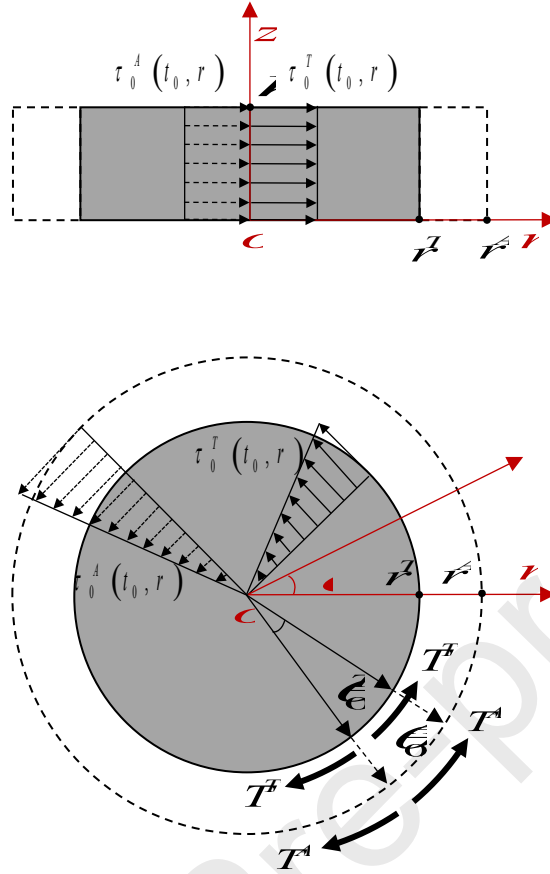
Fig. 3. Distribution of shear strain/shear stress in the intact asphalt binder and the apparent asphalt binder when performing a strain-controlled rotational load

Therefore, the apparent shear strain at any position in the apparent asphalt binder can be expressed by:

$$\gamma^A(t,r) = \gamma_0^A(t_0,r)\sin(\omega t) = \frac{\theta_0^A}{h}r\sin(\omega t) = \frac{r}{r^A}\gamma_0^A(t_0,r^A)\sin(\omega t) \tag{1}$$

where $\gamma^A(t,r)$ is the apparent shear strain at loading time t ($t_0 \leq t \leq (t_0 + 2\pi/\omega)$) and a given radius r ($0 \leq r \leq r^A$); $\gamma_0^A(t_0,r)$, $\gamma_0^A(t_0,r^A)$ are apparent shear strain amplitude at loading time t_0 with a given radius r and apparent radius r^A, respectively; ω is loading frequency; θ_0^A is amplitude of apparent rotational angle; and h is height of the asphalt binder specimen.

The apparent shear stress at any position in the apparent asphalt binder can be modeled

10

as below:

$$\tau^A(t,r) = \tau_0^A(t_0,r)\sin(\omega t + \delta^A) = \frac{r}{r^A}\tau_0^A(t_0,r^A)\sin(\omega t + \delta^A) \qquad (2)$$

in which $\tau^A(t,r)$ is the apparent shear stress at the loading time t and a given radius r; $\tau_0^A(t_0,r)$, $\tau_0^A(t_0,r^A)$ are apparent shear stress amplitude at the loading time t_0 with a given radius r and apparent radius r^A, respectively; and δ^A is apparent phase angle. The apparent shear modulus of the apparent asphalt binder can be calculated by:

$$\left|G^{*A}\right| = \frac{\tau_0^A(t_0,r)}{\gamma_0^A(t_0,r)} \qquad (3)$$

Similarly, the true shear strain at any position in the intact asphalt binder is expressed by:

$$\gamma^T(t,r) = \gamma_0^T(t_0,r)\sin(\omega t) = \frac{\theta_0^T}{h}r\sin(\omega t) = \frac{r}{r^A}\gamma_0^T(t_0,r^T)\sin(\omega t) \qquad (4)$$

where $\gamma^T(t,r)$ is the true shear strain at the loading time t and a given radius r ($0 \le r \le r^T$); $\gamma_0^T(t_0,r), \gamma_0^T(t_0,r^T)$ are true shear strain amplitude at the loading time t_0 for a given radius r and true radius r^T, respectively; and θ_0^T is amplitude of true rotational angle.

The true shear stress at any position in the intact asphalt binder is formulated as follows:

$$\tau^T(t,r) = \tau_0^T(t_0,r)\sin(\omega t + \delta^T) = \frac{r}{r^A}\tau_0^T(t_0,r^T)\sin(\omega t + \delta^T) \qquad (5)$$

in which $\tau^T(t,r)$ is the true shear stress; $\tau_0^T(t_0,r), \tau_0^T(t_0,r^T)$ are true shear stress amplitude at the loading time t_0 for a given radius r and true radius r^T, respectively; and δ^T is true phase angle.

The true shear modulus of the intact asphalt binder can be calculated by:

$$\left|G^{*T}\right| = \frac{\tau_0^T(t_0,r)}{\gamma_0^T(t_0,r)} \qquad (6)$$

The apparent shear strain, apparent shear stress, true shear strain and true shear stress (detailed derivation of the true shear strain and stress are shown in Appendix A) at any

position and any loading time can be obtained. Taking the apparent strain, apparent stress at a given radius r^A, and the true strain, true stress at a given radius r^T in a loading cycle as an example, which is shown in Fig. 4. Two observations can be obtained: (1) the true shear stress amplitude is larger than the apparent shear stress amplitude; and (2) the true shear strain amplitude is smaller than the apparent shear strain amplitude. This is because the apparent shear modulus decreases with the loading time and the true shear modulus does not change with the loading time when performing the time sweep test.
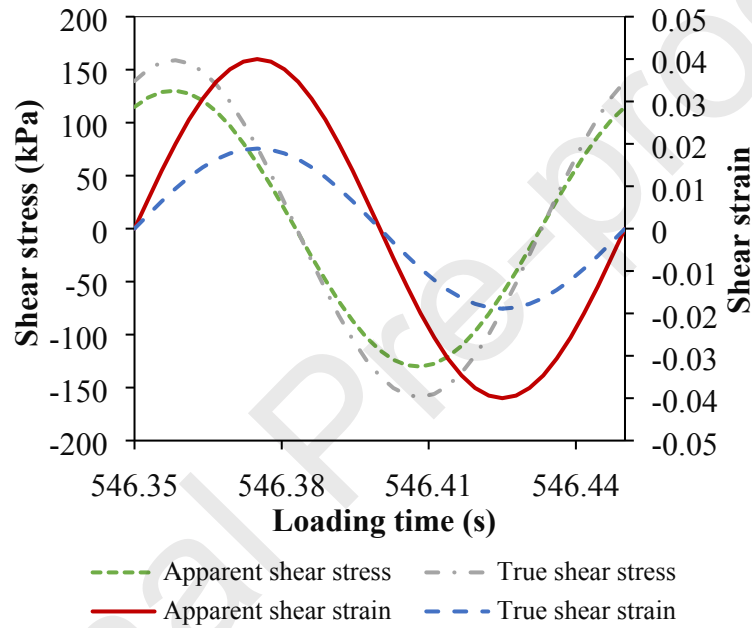
Fig. 4. Apparent strain, apparent stress at a given radius r^A and true strain, true stress at a given radius r^T in a loading cycle

3.2 Establishment of Deterministic Fatigue Damage Model for Asphalt Binders

An EBM approach were proposed to determine the evolution of damage or healing of asphalt mixtures [31], [32], [33], [34], [35]. In this study, the EBM approach can be applied to determine a damage evolution model for asphalt binders. A torque equilibrium principle and two energy balance principles are listed as follows [36][37]:

$$T^A(t_0) = T^T(t_0) \tag{7}$$

$$DSE^A(t_0) = DSE^T(t_0) \tag{8}$$

12

$$RSE^{A}\left(t_{0}\right) = RSE^{T}\left(t_{0}\right) \tag{9}$$

where $T^{A}(t_0)$ is total apparent torque at the loading time t_0; $T^{T}(t_0)$ is total true torque at the loading time t_0; $DSE^{A}(t_0)$ is total apparent dissipated strain energy at the loading time t_0; $DSE^{T}(t_0)$ is total true dissipated strain energy at the loading time t_0; $RSE^{A}(t_0)$ is total apparent recoverable strain energy at the loading time t_0; and $RSE^{T}(t_0)$ is total true recoverable strain energy at the loading time t_0.
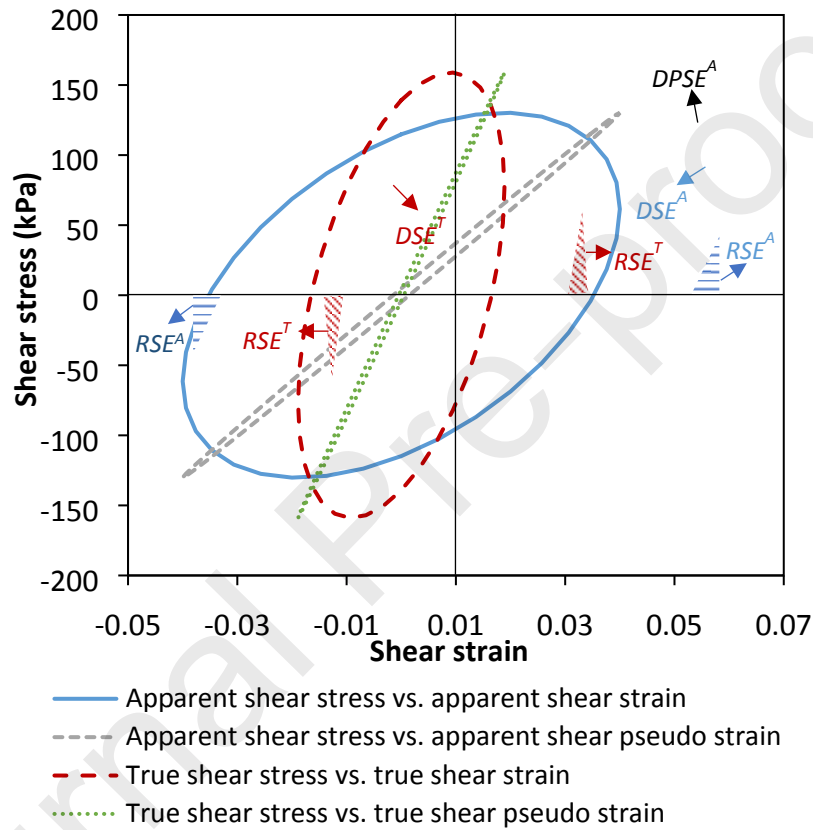
Fig. 5. Energy hysteresis loop of the asphalt binder when performing a strain-controlled shear load

Fig. 5 presents energy hysteresis loop of the asphalt binder when performing a strain-controlled shear load. It consists of four hysteretic loops: (1) apparent shear stress vs. apparent shear strain; (2) apparent shear stress vs. apparent shear pseudo strain; (3) true shear stress vs. true shear strain; and (4) true shear stress vs. true shear pseudo strain. DSE^{A} stands for the apparent dissipated strain energy at any position in the apparent asphalt binder (an area of hysteresis loop (1)); RSE^{A} is the apparent recoverable strain

13

energy at any position in the apparent asphalt binder (an area of two parts filled with horizontal lines in Fig. 5); $DPSE^A$ is apparent dissipated pseudo strain energy at any position in the apparent asphalt binder (an area of hysteresis loop (2)); DSE^T is the true dissipated strain energy at any position in the intact asphalt binder (an area of hysteresis loop (3)); RSE^T stands for the true recoverable strain energy at any position in the intact asphalt binder (an area of two parts filled with diagonal lines in Fig. 5).

However, the two energy balance principles (Eqs. (8) and (9)) just apply to a total energy in the entire volume of the asphalt binder. Therefore, the total energy items should be determined first. For the apparent asphalt binder, the $DSE^A(t_0)$ can obtained as below:

$$DSE^A\left(t_0\right)=\iiint_{V^A}\left[\int_{t_0}^{t_0+2\pi/\omega}\tau^A\left(t,r\right)d\gamma^A\left(t,r\right)\right]dV \tag{10}$$

where V^A is the entire volume of the apparent asphalt binder sample.

The $RSE^A(t_0)$ is calculated by:

$$RSE^A\left(t_0\right)=\iiint_{V^A}\left[\int_{t_0+\left(\pi-\delta^A\right)/\omega}^{t_0+\pi/\omega}+\int_{t_0+\left(2\pi-\delta^A\right)/\omega}^{t_0+2\pi/\omega}\tau^A\left(t,r\right)d\gamma^A\left(t,r\right)\right]dV \tag{11}$$

Similarly, for the intact asphalt binder, the $DSE^T(t_0)$ is calculated as follows:

$$DSE^T\left(t_0\right)=\iiint_{V^T}\left[\int_{t_0}^{t_0+2\pi/\omega}\tau^T\left(t,r\right)d\gamma^T\left(t,r\right)\right]dV \tag{12}$$

where V^T is the entire volume of the intact asphalt binder sample.

The $RSE^T(t_0)$ can be determined by the following equation:

$$RSE^T\left(t_0\right)=\iiint_{V^T}\left[\int_{t_0+\left(\pi-\delta^T\right)/\omega}^{t_0+\pi/\omega}+\int_{t_0+\left(2\pi-\delta^T\right)/\omega}^{t_0+2\pi/\omega}\tau^T\left(t,r\right)d\gamma^T\left(t,r\right)\right]dV \tag{13}$$

The $T^A(t_0)$ is calculated as below:

$$T^A\left(t_0\right)=\int_0^{r^A}\tau_0^A\left(t,r\right)\cdot2\pi r^2dr \tag{14}$$

Similarly, the $T^T(t_0)$ can be determined by:

$$T^T\left(t_0\right)=\int_0^{r^T}\tau_0^T\left(t,r\right)\cdot2\pi r^2dr \tag{15}$$

Substitute Eqs. (14), (15) into Eq (7), damage density of the asphalt binder can be

14

defined and calculated by the following expression (detailed derivation is shown in the Appendix A):

$$\phi = 1 - \frac{\pi \left(r^T \right)^2}{\pi \left(r^A \right)^2} = 1 - \sqrt{\frac{\left| G^{*A} \right|}{\left| G^{*T} \right|}} \qquad (16)$$

where ϕ is the damage density of the asphalt binder. In this study, the damage density represents the proportion of failure area to total area of the asphalt binder sample when performing a strain-controlled shear load.

A pseudo J-integral Paris' law model for fatigue cracking in asphalt mixtures and pavements was proposed [38], [39]. In this study, the pseudo J-integral Paris' law model is used to formulate the deterministic damage evolution rate for asphalt binders, which is shown as below [38], [39]:

$$\frac{d\phi}{dt} = A \left(J_R \right)^n \qquad (17)$$

where A and n are Paris's law coefficients associated with damage evolution rate, which are intrinsic parameters of the material; J_R is pseudo J-integral, which can be calculated by:

$$J_R = \frac{\partial \left[\int_0^t DPSE^A \left(t_0 \right) dt_0 \right]}{\partial \left(S^c \right)} = \frac{\partial \left[\int_0^t DPSE^A \left(t_0 \right) dt_0 \right] / \partial t}{\partial \left(S^c \right) / \partial t} = \frac{DPSE^A \left(t \right)}{\partial \left(S^c \right) / \partial t} \qquad (18)$$

in which $DPSE^A(t)$ is the total dissipated pseudo strain energy at loading time t of the asphalt binder; S^c is crack area of the asphalt binder, which is calculated by:

$$\frac{\partial S^c}{\partial t} = \frac{\partial \left[\pi \left(r^A \right)^2 \phi \right]}{\partial t} = \pi \left(r^A \right)^2 \frac{\partial \phi}{\partial t} \qquad (19)$$

The $DPSE^A(t)$ at any loading time t can be calculated as follows:

$$DPSE^A \left(t \right) = \iiint_{V^A} \left[\int_t^{t+2\pi/\omega} \tau^A \left(t, r \right) d\gamma_R^A \left(t, r \right) \right] dV \qquad (20)$$

in which $\gamma_R^A \left(t, r \right)$ is apparent pseudo strain at the loading time t and a given radius r. Substitute Eq. (18), Eq. (19), Eq. (20) into Eq. (17), damage evolution rate of the asphalt

binder can be determined (detailed derivation is given in Appendix B). The expression of the damage evolution rate can be obtained as below:

$$\frac{d\phi}{dt} = A^{1/(n+1)} \left[\frac{1}{2}\pi h \left| G^{*A} \right| \left[\gamma_0^A\left(t, r^A\right) \right]^2 \sin\left(\delta^A - \delta_{NLVE}^A\right) \right]^{n/(n+1)} \tag{21}$$

in which δ_{NLVE}^A is apparent phase angle at a critical nonlinear viscoelastic point of the asphalt binder.

Finally, substitute Eq. (16) into Eq. (21), the deterministic damage evolution rate model can be defined by the following expression:

$$\frac{d\phi}{dt} = a\left[f\left(\delta^A, \phi\right) \right]^b \tag{22}$$

where $\quad f\left(\delta^A, \phi\right) = \frac{1}{2}\pi h \left| G^{*T} \right| \gamma_0^A\left(t, r^A\right)\left(1-\phi\right)^2 \sin\left(\delta^A - \delta_{NLVE}^A\right); \quad a = A^{1/(n+1)};$

$b = n/(n+1)$. $\left| G^{*T} \right|$, $\gamma_0^A\left(t, r^A\right)$, δ_{NLVE}^A, a, b, h are constants and δ^A, ϕ are variables in $f\left(\delta^A, \phi\right)$.

3.3 Analysis of Variability for Fatigue Damage Results

Substituting the time sweep test data into Eq. (16) and Eq. (21), the damage density and damage evolution rate of the asphalt binder can be obtained as shown in Fig. 6. Four observations can be obtained: (1) the damage density increases and damage evolution rate decreases with the increase of loading time (in Fig. 6a); (2) the damage evolution rate decreases with the increase of damage density (in Fig. 6b); (3) the damage density of all asphalt binder samples fluctuates in a certain range at a fixed loading time, or loading time of all asphalt binder samples fluctuates in a certain range at a fixed damage density (in Fig. 6a); and (4) the variability of damage density in asphalt binder samples (indicated by the red distribution) decreases over time, and the variability of loading time at a fixed damage density (indicated by blue distribution) increases over time (in Fig. 6a).

16
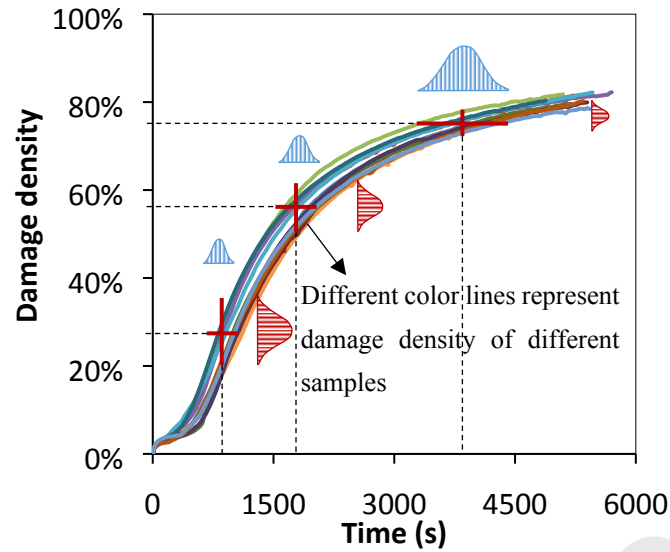
a. Relationship between the damage density and loading time among different

asphalt binder samples
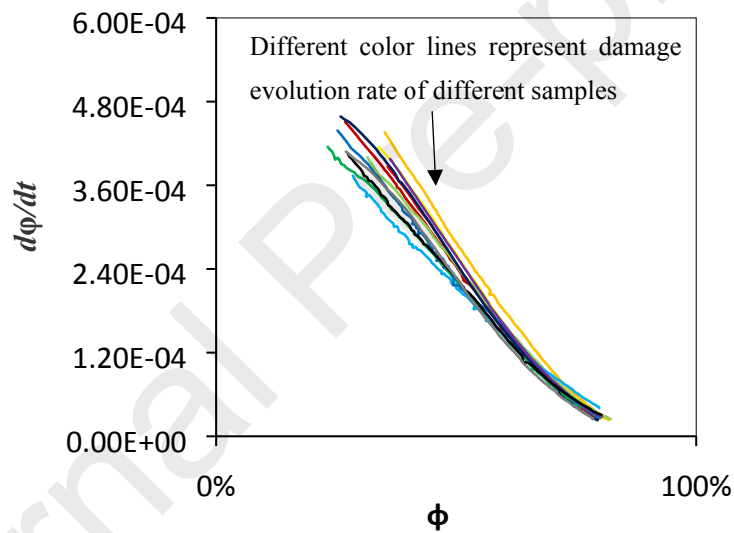
b. Relationship between the damage evolution rate and the damage density among

different asphalt binder samples

Fig. 6. Calculation results of the damage density and damage evolution rate among

different asphalt binder samples

The reason for the observation (1) and (2) is that the energy dissipation increases with

the loading time which makes damage density increases, and the energy dissipation

increase rate decreases with the loading time which makes damage evolution rate

decreases when performing a shear strain-controlled time sweep test. The similar cyclic

17

energy-dissipation behavior has been analyzed in metals [40][41]. For the observation (3), it is caused by many different uncertainties, such as simplified assumptions made for internal damage process, material properties, microstructure heterogeneity and others. The reason for the observation (4) is that the damage evolution rate gradually slows down with the increase of loading time. Hence, the damage density and damage evolution rate of all asphalt binder samples have a similar evolution trend but not exactly same under the same loading condition (the same oscillation shear strain level, temperature, loading frequency). In other words, the results of damage density and damage evolution rate among different asphalt binder samples exhibit the characteristics of variability even under the same loading condition.

However, the damage density (Eq. (16)) and damage evolution rate (Eq. (21)) established in section 3.2 are deterministic models, which means that the uncertainties are not considered. To overcome this problem, the probability analysis is introduced first. Fig. 7 presents sketch of the probability distribution of the damage density and the corresponding loading time. The area "NPM" represents the probability of the damage density $\phi(t)$ less than a given damage density ϕ, which is defined as $P\{\phi(t)<\phi\}$. The area "LPQ" represents the probability of the loading time $t(\phi)$ larger than a given loading time t, which is defined as $P\{t(\phi)>t\}$. $\phi(t)$ and $t(\phi)$ are the abscissa and ordinate of point P in Fig. 7, which represents any damage density and the corresponding loading time after a time sweep test, respectively. Due to the non-decreasing nature of the process of the damage density, $P\{\phi(t)<\phi\}$ and $P\{t(\phi)>t\}$ have the relationship as follows [23]:

$$P\{t(\phi)>t\} = P\{\phi(t)<\phi\} \tag{23}$$

18
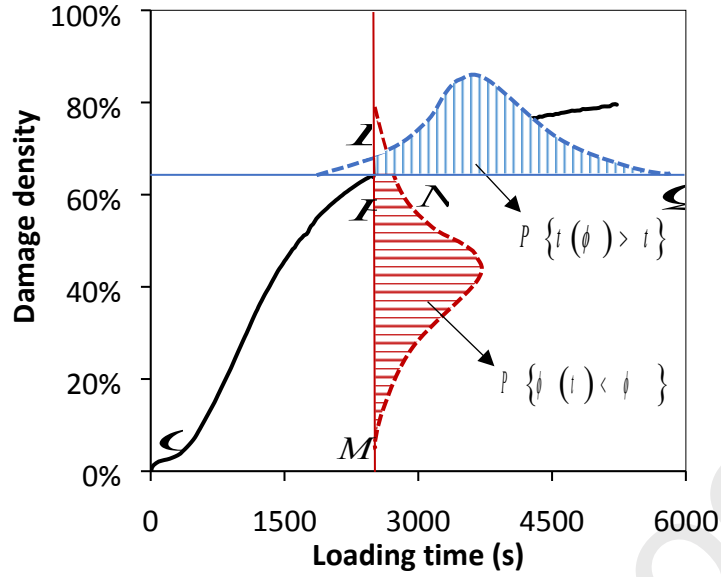
Fig. 6. Sketch of the probability distribution of the damage density and the loading time

4 Determination of Stochastic Fatigue Damage Model for Asphalt Binders

According to the analysis results above, the variability of fatigue damage does exist. To add the variability into the deterministic fatigue damage model, the stochastic fatigue damage model can be proposed for the asphalt binder in this section. This section contains the following three aspects:

(1) Add a random variable into the deterministic damage evolution rate model to randomize the model;

(2) Estimate model parameters based on the maximum likelihood estimation; and

(3) Determine the stochastic damage model coupling variability and fatigue damage mechanism for the asphalt binder.

4.1 Randomization of the Deterministic Damage Evolution Rate Model

First, a random variable $X(t)$ is added into the deterministic damage evolution rate model (Eq. (22)), which is presented as follows [42]:

$$\frac{d\phi}{dt} = X(t)a\left[f\left(\delta^A,\phi\right)\right]^b \tag{24}$$

Mathematical transformation is made for Eq. (24), which yields:

19

$$\ln X(t) = \ln \frac{d\phi}{dt} - \ln a - b \ln \left[f\left(\delta^A, \phi\right) \right] \tag{25}$$

Assume that the random variable $Y(t) = \ln X(t)$ obeys a normal distribution, hence, the random variable $X(t)$ obeys a logarithmic normal distribution. The relationship of mathematical expectation of $Y(t)$ and $X(t)$ is shown as follows:

$$\mu_X = \exp\left(\mu_Y + \sigma_Y^2/2\right) \tag{26}$$

where μ_Y is mathematical expectation of $Y(t)$; σ_Y^2 is variance of $Y(t)$; μ_X is mathematical expectation of $X(t)$.

The relationship between the variance of $Y(t)$ and $X(t)$ is obtained as below:

$$\sigma_X^2 = \exp\left(2\mu_Y + \sigma_Y^2\right)\left(\exp\left(\sigma_Y^2\right) - 1\right) \tag{27}$$

in which σ_X^2 is the variance of $X(t)$.

In addition, Yang and Manning suggested that μ_X of $X(t)$ is equal to 1.0 [22]. Substitute $\mu_X = 1.0$ into Eq. (26) and Eq. (27), σ_Y^2 can be calculated by the following expression:

$$\sigma_Y^2 = \ln\left(\sigma_X^2 + 1\right) \tag{28}$$

Combine Eq. (26) with Eq. (28), the expression of μ_Y is obtained as below:

$$\mu_Y = -\ln^2\left(\sigma_X^2 + 1\right)/2 \tag{29}$$

Then, perform an integration for Eq. (24), which yields:

$$\int_0^{\phi(t)} \frac{d\phi}{a\left[f\left(\delta^A, \phi\right)\right]^b} = \int_0^{t(\phi)} X(t)dt \tag{30}$$

The random variable $W = \int_0^{t(\phi)} X(t)dt$ is assumed as a logarithmic normal distribution. In this way, the random variable $Z = \ln W$ obeys the normal distribution. According to the relationship of the logarithmic normal distribution and the corresponding normal distribution, the variance of $Z(t)$ can be represented by mathematical expectation and variance of $W(t)$, the expression is presented as below:

$$\sigma_Z^2 = \ln\left(\sigma_W^2/\mu_W^2 + 1\right) \tag{31}$$

where σ_Z^2 is variance of $Z(t)$; μ_W is mathematical expectation of $W(t)$; σ_W^2 is variance of $W(t)$.

The mathematical expectation of $Z(t)$ also can be represented by μ_W and σ_W^2, which gives:

$$\mu_Z = \ln\left[\mu_W/\sqrt{\left(\sigma_W^2/\mu_W^2 + 1\right)}\right] \tag{32}$$

in which μ_Z is mathematical expectation of $Z(t)$.

In addition, to obtain σ_Z^2 and μ_Z, the key is calculating μ_W and σ_W^2, and the mathematical expectation μ_W can be determined as follows:

$$\mu_W = \int_{-\infty}^{x} dx \int_0^t X(t)\,dt = \int_0^t \int_{-\infty}^{x} X(t)\,dx\,dt = \mu_X t \tag{33}$$

The variance of random variable $Z(t)$ can be calculated as below:

$$\sigma_Z^2 = \int_0^t \int_0^t Cov\left(X(t_1), X(t_2)\right) dt_1 dt_2 \tag{34}$$

where $Cov\left(X(t_1), X(t_2)\right)$ is an auto-covariance.

From the physical standpoint, the auto-covariance function of the damage evolution rate should decrease as the difference between two time t_1 and t_2 increases. The general auto-covariance function of the following form is assumed for the random process $X(t)$ [42]:

$$Cov\left(X(t_1), X(t_2)\right) = \sigma_X^2 \exp\left(-\varsigma|t_2 - t_1|\right) \tag{35}$$

where ς^{-1} indicates a measure of the correlation time for $X(t)$ and will be called "correlation time" hereafter for simplicity.

The value of the correlation time ς^{-1} is used to match the probability distribution in the following section. Finally, substitute Eq. (35) to Eq. (34) and carry out the integration, which yields:

$$\sigma_W^2 = \beta^2 \sigma_X^2 \tag{36}$$

21

in which $\beta = \sqrt{[\exp(-\varsigma t) + \varsigma t - 1]/2}$.

4.2 Estimation of Model Parameters

To determine the stochastic damage model, it is necessary to solve three model parameters a, b and σ_X^2 first. In this study, a maximum likelihood estimation approach is performed to solve these model parameters. The probability density function of the random variable $X(t)$ is presented as below:

$$f(x) = \begin{cases} \dfrac{1}{\sqrt{2\pi}\sigma_X x} \exp\left[-(\ln x - \mu_X)^2/(2\sigma_X^2)\right] & x \ge 0 \\ 0 & x < 0 \end{cases} \tag{37}$$

A likelihood function of the test data is given by:

$$L\left(x_1, x_2, \cdots, x_i, \cdots x_M; a, b, \sigma_X^2\right) = \prod_{i=1}^{M} \frac{1}{\sqrt{2\pi}x_i\sigma_X} \exp\left(-(\ln x_i - \mu_X)^2/(2\sigma_X^2)\right) \tag{38}$$

where $L\left(x_1, x_2, \cdots, x_i, \cdots x_M; a, b, \sigma_X^2\right)$ is likelihood function; $x_1, x_2, \cdots, x_i, \cdots x_M$ are sample of the random variable $X(t)$.

The model parameters a, b and σ_X^2 can be obtained by numerically maximizing the logarithm of Eq. (38). Take the logarithm of both sides of Eq. (38), which gives:

$$\ln L\left(x_1, x_2, \cdots x_M; a, b, \sigma_X^2\right) = \sum_{i=1}^{M} \ln\left[\frac{1}{\sqrt{2\pi}x_i\sigma_X} \exp\left(-(\ln x_i - \mu_X)^2/(2\sigma_X^2)\right)\right] \tag{39}$$

According to test data of any sample i and Eq. (25), the following equation can be obtained:

$$\ln x_i = \ln \frac{d\phi_i}{dt} - \ln a - b\ln\left[f\left(\delta_i^A, \phi_i\right)\right] \tag{40}$$

Then, substitute Eq. (40) into Eq. (39), and perform the partial derivative of the parameter a. Set the partial derivatives to zero, which gives:

$$\ln a + \frac{b}{M}\sum_{i=1}^{M} \ln\left[f\left(\delta_i^A, \phi_i\right)\right] - \frac{1}{M}\sum_{i=1}^{M}\left(\ln\frac{d\phi_i}{dt} - \mu_X\right) - \sigma_X^2 = 0 \tag{41}$$

Perform the partial derivative of the parameter b and set it to zero, yielding:

$$\frac{1}{M}\sum_{i=1}^{M}\left[\ln\left[f\left(\delta_i^A,\phi_i\right)\right]\left[\sigma_X^2+\ln\frac{d\phi_i}{dt}-\ln a-b\ln\left[f\left(\delta_i^A,\phi_i\right)\right]-\mu_X\right]\right]=0 \qquad (42)$$

Similarly, take the partial derivative of the variance σ_X^2, giving:

$$\sigma_X^2-\frac{1}{M}\sum_{i=1}^{M}\left[\ln\frac{d\phi_i}{dt}-\ln a-b\ln\left[f\left(\delta_i^A,\phi_i\right)\right]-\mu_X\right]^2=0 \qquad (43)$$

Then, combine Eq. (41), Eq. (42) with Eq. (43), the expression of the parameter b can be calculated by:

$$b=\frac{\dfrac{1}{M}\sum_{i=1}^{M}\ln\left[f\left(\delta_i^A,\phi_i\right)\right]\dfrac{1}{M}\sum_{i=1}^{M}\ln\dfrac{d\phi_i}{dt}-\dfrac{1}{M}\sum_{i=1}^{M}\ln\left[f\left(\delta_i^A,\phi_i\right)\right]\ln\dfrac{d\phi_i}{dt}}{\left[\dfrac{1}{M}\sum_{i=1}^{M}\ln\left[f\left(\delta_i^A,\phi_i\right)\right]\right]^2-\dfrac{1}{M}\sum_{i=1}^{M}\ln^2\left[f\left(\delta_i^A,\phi_i\right)\right]} \qquad (44)$$

The parameter a can be determined by the following mono basic quadratic equation:

$$\begin{aligned}
&\ln^2 a+\ln a\left(1-\frac{2}{M}\sum_{i=1}^{M}\ln\frac{d\phi_i}{dt}+\frac{2b}{M}\sum_{i=1}^{M}\ln\left[f\left(\delta_i^A,\phi_i\right)\right]\right)\\
&+\frac{1}{M}\sum_{i=1}^{M}\ln^2\frac{d\phi_i}{dt}+\frac{b^2}{M}\sum_{i=1}^{M}\ln^2\left[f\left(\delta_i^A,\phi_i\right)\right]-\frac{2b}{M}\sum_{i=1}^{M}\ln\left[f\left(\delta_i^A,\phi_i\right)\right]\ln\frac{d\phi_i}{dt}\\
&-\frac{1}{M}\sum_{i=1}^{M}\ln\frac{d\phi_i}{dt}+\frac{b}{M}\sum_{i=1}^{M}\ln\left[f\left(\delta_i^A,\phi_i\right)\right]=0
\end{aligned} \qquad (45)$$

Finally, the variance σ_X^2 of random variable $X(t)$ can be obtained:

$$\sigma_X^2=\ln a+\frac{b}{M}\sum_{i=1}^{M}\ln\left[f\left(\delta_i^A,\phi_i\right)\right]-\frac{1}{M}\sum_{i=1}^{M}\left(\ln\frac{d\phi_i}{dt}-\mu_X\right)=0 \qquad (46)$$

Calculated results of the parameters a, b and the variance σ_X^2 of the random variable $X(t)$ are shown in Fig. 8. It is found that parameters a, b and σ_X^2 become stable with the increase of the number of samples. It indicates that the stability and reliability of model parameters determined by the maximum likelihood estimation approach can be improved by increasing of the number of samples. The change trend of the parameters a, b and the variance σ_X^2 is similar, which shows the estimation error caused by the number of samples is consistent for any estimated parameter.
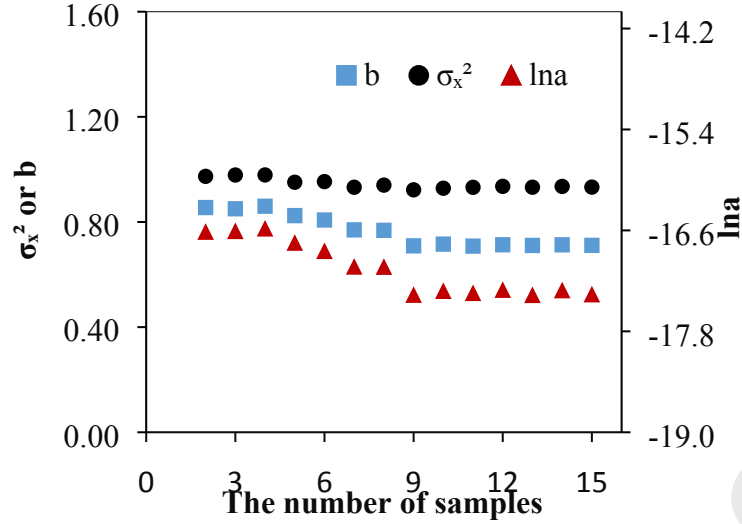
Fig. 8. Calculated results of parameters *a*, *b* and the variance σ_X^2 of the random

variable *X(t)*

4.3 Establishment of Stochastic Damage Model

Since the random variable $Z = \ln W$ obeys the normal distribution, a cumulative

distribution function of loading time (TCDF) can be determined by the following

expression:

$$P\{t(\phi) \le t\} = \Phi\left\{\left[\mu_Z(t) - \ln \overline{t}\right] / \sigma_Z(t)\right\} \tag{47}$$

where $P\{t(\phi) \le t\}$ is defined as the TCDF; $\Phi\{\cdot\}$ is cumulative distribution function

of the standard normal distribution; $\overline{t}$ is mean value of the loading time at a given

mean value of the damage density $\overline{\phi}$; $\mu_Z(t)$ is mathematical expectation of random

variable of *Z(t)* at any loading time; $\sigma_Z(t)$ is variance of random variable of *Z(t)* at

any loading time.

Next, combine Eq. (23) with Eq. (47), the DDEP can be obtained as below:

$$P\{\phi(t) \le \phi\} = P\{t(\phi) \ge t\} = 1 - P\{t(\phi) \le t\} = 1 - \Phi\left\{\left[\mu_Z(t) - \ln \overline{t}\right] / \sigma_Z(t)\right\} \tag{48}$$

where $P\{\phi(t) \le \phi\}$ is defined as the DDEP.

If the two functions $\mu_Z(t)$, $\sigma_Z(t)$ and the mean value of the loading time $\overline{t}$ are

obtained, the TCDF (Eq. (47)) and the DDEP (Eq. (48)) will be determined. The specific procedure to establish a stochastic damage model is elaborated below step by step.

Step 1: Formulate $\mu_Z(t)$, $\sigma_Z(t)$ **and** $\overline{t}$

Substitute Eq. (38), Eq. (41) into Eq. (37). $\mu_Z(t)$ can be calculated by:

$$\mu_Z(t) = \ln(t) - \frac{1}{2}\ln\left[\beta^2/t^2\left[\exp\left[\ln^2\left(\sqrt{\sigma_X^2 + 1}\right)\right] - 1\right] + 1\right] \tag{49}$$

Then, the variance $\sigma_Z(t)$ can be determined as below:

$$\sigma_Z(t) = \sqrt{\ln\left[\beta^2/t^2\left[\exp\left[\ln^2\left(\sqrt{\sigma_X^2 + 1}\right)\right] - 1\right] + 1\right]} \tag{50}$$

Next, there is a one-to-one correspondence between the damage density $\overline{\phi}$ and the loading time $\overline{t}$ in the deterministic damage model. When the damage density $\overline{\phi}$ is fixed, the corresponding loading time $\overline{t}$ can be calculated, and vice versa. The expression of the loading time $\overline{t}$ is shown as below:

$$\overline{t} = \int_0^{\overline{\phi}} \frac{d\phi}{a\left[f\left(\delta^A, \phi\right)\right]^b} = \frac{1 - \left[1 - \overline{\phi}\right]^{1-2b}}{a(1-2b)\left[\sin\left(\delta^A - \delta_{NLVE}^A\right)\right]^b} \tag{51}$$

Fig. 9 presents comparison between the test data and calculated result of the mean value of the loading time at different damage densities. It indicates that the calculated results match the test data well. In addition, the mean value of the loading time increases with the increase of damage density and the growth rate increases with the increase of the damage density. That is because longer loading time is required to produce the energy to promote the same increase of damage density when performing a shear-controlled test.
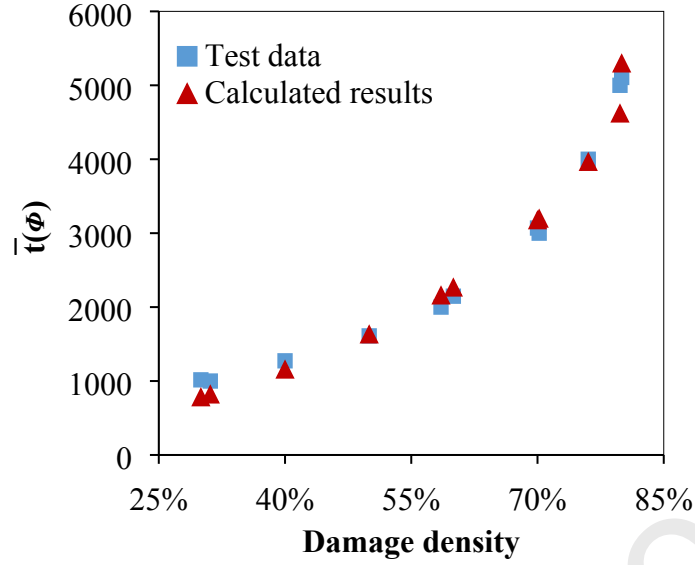
Fig. 9. Comparison between the test data and calculated results of the mean value of

the loading time at different damage density values

Step 2: Determine Cumulative Distribution Function of Loading Time **and** Damage

Density Exceedance Probability

If the β is determined by the correlation time ς^{-1}, $\mu_Z(t)$ and $\sigma_Z^2(t)$ will be

obtained based on Eqs. (49) and (50). Hence, the correlation time ς^{-1} is critical for

determining the TCDF and DDEP. There are two extreme cases discussed as examples

[23]:

(1) when the correlation time ς^{-1} is approaches to zero, the β can be determined by:

$$\lim_{\varsigma^{-1} \to 0} \beta = \lim_{\varsigma^{-1} \to 0} \frac{t\left(1 - e^{-\varsigma t}\right)}{\sqrt{2\left(e^{-\varsigma t} + \varsigma t - 1\right)}} = 0 \tag{52}$$

In this case, the damage evolution of the asphalt binder is a lognormal white noise

random process. In this case, there is no statistical dispersion for the damage evolution,

which is the least conservative case.

(2) when the correlation time ς^{-1} is approaches to infinite, the β can be calculated

by:

$$\lim_{\varsigma^{-1}\to\infty}\beta = \lim_{\varsigma^{-1}\to 0}\frac{\sqrt{2\left(1-\varsigma t+\varsigma^2 t^2/2-o\left(\varsigma^3 t^3\right)+\varsigma t-1\right)}}{\varsigma}=t \tag{53}$$

Under the circumstances, the variability of the damage evolution of the asphalt binder is the greatest, which is the most conservative case.

In this study, the TCDF and DDEP are determined by different correlation time between these two extreme examples. Fig. 10a and 10b present that the TCDF and DDEP are calculated by some different correlation times ($10^6, 10^3, 10^2, 10^1, 10^{-1}, 10^{-6}$). The TCDF and DDEP gradually flatten out with increase of the correlation time. The TCDF and DDEP are close to a no statistical dispersion process when the correlation time is small (10^{-6}). The variability of the TCDF and DDEP are larger when the correlation time is 10^6. They are consistent with the analysis of Eq. (52) and Eq. (53).

Next, an appropriate correlation time is adapted to match the TCDF and DDEP with the discrete test results. Fig. 10c and 10d show that the matching curve between test results and the TCDF and DDEP. Besides, Fig. 10e and 10f show the comparison between test results and the TCDF at different damage density (30%, 40% 50%, 60%, 70%, 80%) and the DDEP at different loading time (1000s, 2000s, 3000s, 4000s, 5000s), respectively. It can be seen from Fig. 10e and 10f that the TCDF and DDEP match the test results well. The TCDF increases with increase of the loading time at a given damage density, and the variability of damage density decreases with increase of the loading time, while the change trend of the DDEP is opposite. These analysis results are consistent with the variability of the damage density shown in Fig. 6a.
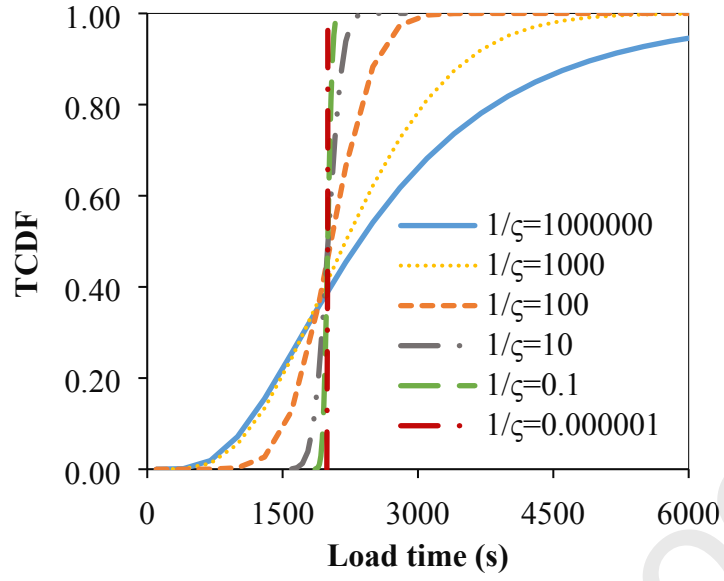
a. TCDF at different correlation time
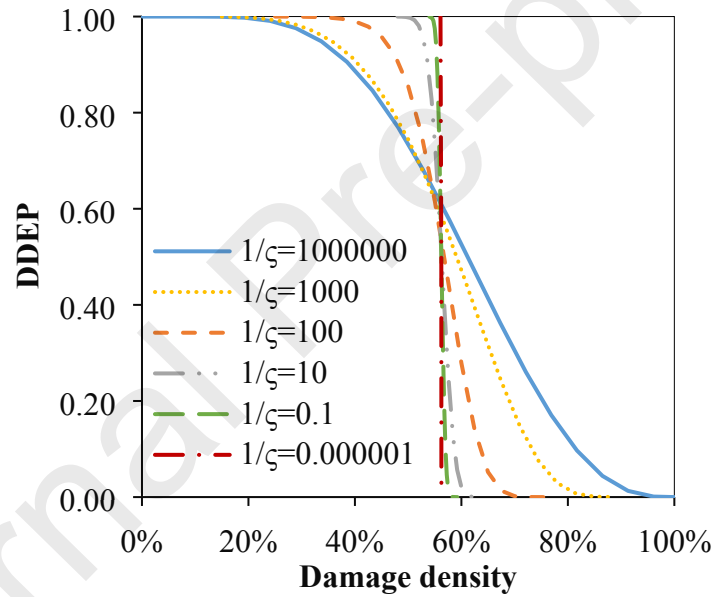
b. DDEP at different correlation time
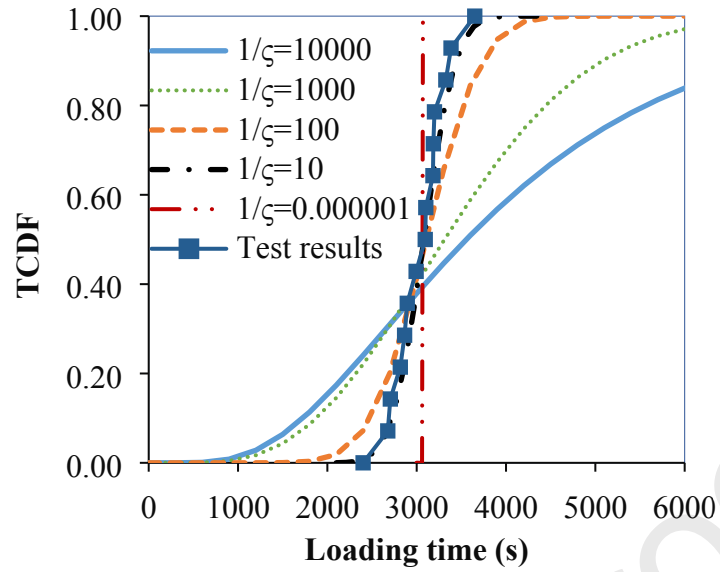
c. Matching curve between test results and the TCDF
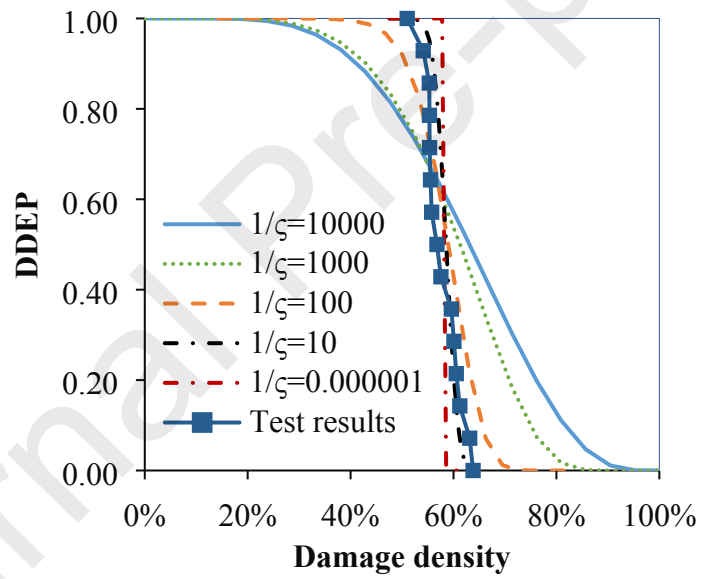
d. Matching curve between test results and the DDEP
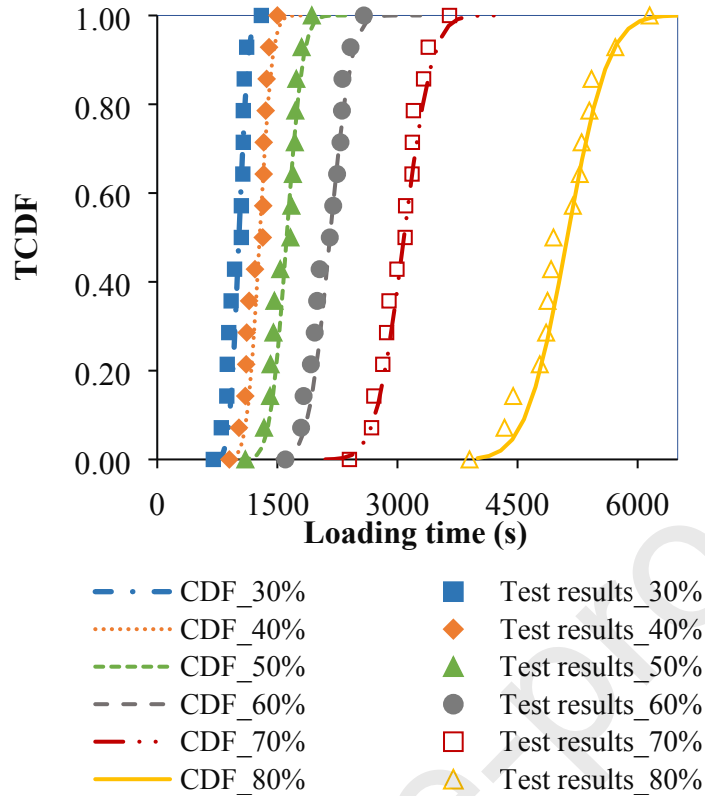
e. Comparison between test results and the TCDF at different damage density
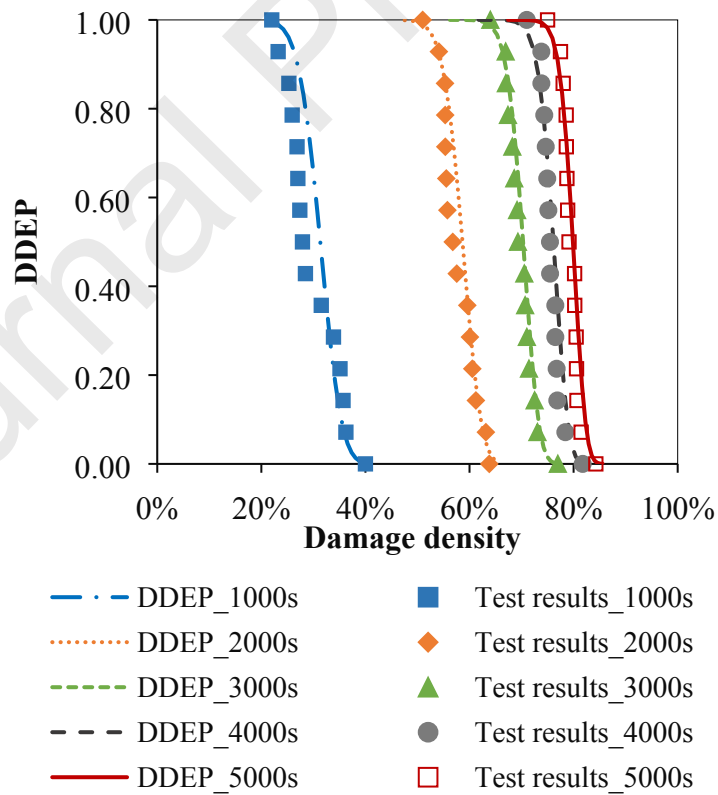
f. Comparison between test results and the DDEP at different loading time

Fig. 10. Cumulative distribution function of loading time (TCDF) and damage density

exceedance probability (DDEP) of the asphalt binder

Step 3: Establish stochastic damage model

All of the correlation time parameters determined in Step 2 are plotted in Fig. 11. It is found that there is a linear relationship between the correlation time ς^{-1} and the damage density. The linear relation can be expressed by the following equation:

$$\varsigma^{-1} = k_1\phi + k_2 \tag{54}$$

where k_1 and k_2 are fitting coefficients.
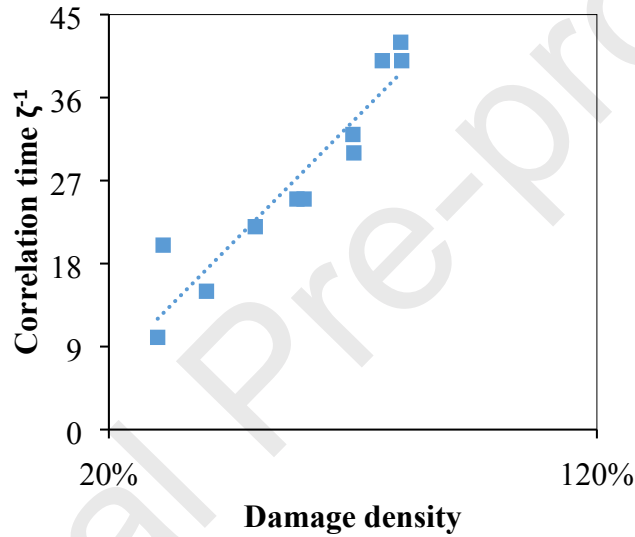
Fig. 11. Relationship between the correlation time and the damage density

Substitute Eqs. (47), (48), (49), (50), (51) into Eq. (54), the stochastic damage model of the asphalt binder can be expressed by:

$$P\{t(\phi) \le t\} = \Phi\left\{f\left(\phi, a, b, \sigma_X{}^2, k_1, k_2\right)\right\} \tag{55}$$

$$P\{\phi(t) \le \phi\} = 1 - \Phi\left\{f\left(\phi, a, b, \sigma_X{}^2, k_1, k_2\right)\right\} \tag{56}$$

in which $f\left(\phi, a, b, \sigma_X{}^2, k_1, k_2\right)$ is a function of $\phi, a, b, \sigma_X{}^2, k_1, k_2$. The variables a, b are the material parameters which is depend on the material and $\sigma_X{}^2, k_1, k_2$ are the variability parameters associate with uncertainty of the damage process.

31

Therefore, if a correlation time ς^{-1} at any damage density is given, the variability of the entire damage evolution process of the asphalt binder could be determined based on Eqs. (55) and (56). In other words, the variability of minor damage of the asphalt binder can be used to predict the variability of severe damage.

5. Conclusions

To address the challenge of coupling the variability and fatigue damage mechanism, a stochastic damage model is proposed to track the variability of the entire fatigue damage process for the viscoelastic materials. A representative viscoelastic material, the asphalt binder, is selected for investigation in this study. The main findings of this study are listed as follows:

- Damage density which represents the proportion of the failure area to the total area of the asphalt binder sample can be determined by the apparent shear modulus and true shear modulus. Damage evolution rate of the asphalt binder is a function of material properties, apparent shear modulus, apparent shear strain amplitude and apparent phase angle.

- Cumulative distribution function of loading time (TCDF) and damage density exceedance probability (DDEP) of the asphalt binder are determined and experimentally verified. The TCDF increases with the loading time at a given damage density, and the variability of damage density decreases with the loading time, while the trend of the DDEP is opposite.

- A stochastic damage model coupled variability and fatigue damage mechanism for the asphalt binder is established and proven to be a function of the damage density, material parameters and variability parameters.

- The variability of the entire damage process of the asphalt binder can be determined by a correlation time at any damage density. Therefore, the variability of a minor damage of the asphalt binder can be used to predict the variability of a severe damage based on the stochastic damage model.

Appendix A. Derivation of Damage Density, True Shear Stress and Shear Strain

The expression of Eq. (10) can be derived as follows:

$$
\begin{aligned}
DSE^A(t_0) &= \iiint_{V^A}\left[\int_{t_0}^{t_0+2\pi/\omega}\tau^A(t,r)\,d\gamma^A(t,r)\right]dV \\
&= \iiint_{V^A}\left[\int_{t_0}^{t_0+2\pi/\omega}\tau_0^A(t_0,r)\sin(\omega t+\delta^A)\,d\left[\gamma_0^A(t_0,r)\sin(\omega t)\right]\right]dV \\
&= \iiint_{V^A}\left[\tau_0^A(t_0,r)\gamma_0^A(t_0,r)\int_{t_0}^{t_0+2\pi/\omega}\sin(\omega t+\delta^A)\cos(\omega t)\,d(\omega t)\right]dV \\
&= \iiint_{V^A}\left[\tau_0^A(t_0,r)\gamma_0^A(t_0,r)\pi\sin(\delta^A)\right]dV \\
&= \int_0^{2\pi}\int_0^{r^A}\int_0^h\left[\frac{r}{r^A}\tau_0^A(t_0,r^A)\frac{r}{r^A}\gamma_0^A(t_0,r^A)\pi\sin(\delta^A)\right]r\,d\theta\,dr\,dz \\
&= 2\pi^2 h\sin(\delta^A)\tau_0^A(t_0,r^A)\gamma_0^A(t_0,r^A)\int_0^{r^A}\left(\frac{r}{r^A}\right)^2 r\,dr \\
&= \frac{1}{2}h\pi^2\left(r^A\right)^2\tau_0^A(t_0,r^A)\gamma_0^A(t_0,r^A)\sin(\delta^A)
\end{aligned}
\tag{A.1}
$$

The expression of Eq. (11) can be derived as below:

$$
\begin{aligned}
RSE^A(t_0) &= \iiint_{V^A}\left[\int_{t_0+(\pi-\delta^A)/\omega}^{t_0+\pi/\omega}+\int_{t_0+(2\pi-\delta^A)/\omega}^{t_0+2\pi/\omega}\tau^A(t,r)\,d\gamma^A(t,r)\right]dV \\
&= \iiint_{V^A}\left[\tau_0^A(t_0,r)\gamma_0^A(t_0,r)\left[\int_{t_0+(\pi-\delta^A)/\omega}^{t_0+\pi/\omega}+\int_{t_0+(2\pi-\delta^A)/\omega}^{t_0+2\pi/\omega}\sin(\omega t+\delta^A)\cos(\omega t)\,d(\omega t)\right]\right]dV \\
&= \int_0^{2\pi}\int_0^{r^A}\int_0^h\left[\frac{r}{r^A}\tau_0^A(t_0,r^A)\frac{r}{r^A}\gamma_0^A(t_0,r^A)\left(\delta^A-\frac{\pi}{2}+\frac{1}{2}\sin(2\delta^A)+\cos^3(\delta^A)\right)\right]r\,d\theta\,dr\,dz \\
&= 2\pi h\left(\delta^A-\frac{\pi}{2}+\frac{1}{2}\sin(2\delta^A)+\cos^3(\delta^A)\right)\tau_0^A(t_0,r^A)\gamma_0^A(t_0,r^A)\int_0^{r^A}\left(\frac{r}{r^A}\right)^2 r\,dr \\
&= \frac{1}{2}h\pi\left(r^A\right)^2\left(\delta^A-\frac{\pi}{2}+\frac{1}{2}\sin(2\delta^A)+\cos^3(\delta^A)\right)\tau_0^A(t_0,r^A)\gamma_0^A(t_0,r^A)
\end{aligned}
$$

$$\tag{A.2}$$

Similarly, the expression of Eqs. (12) and (13) can be obtained:

$$
DSE^T(t_0)=\frac{1}{2}h\pi^2\left(r^T\right)^2\tau_0^T(t_0,r^T)\gamma_0^T(t_0,r^T)\sin(\delta^T)
\tag{A.3}
$$

$$
RSE^T(t_0)=\frac{1}{2}h\pi\left(r^T\right)^2\left(\delta^T-\frac{\pi}{2}+\frac{1}{2}\sin(2\delta^T)+\cos^3(\delta^T)\right)\tau_0^T(t_0,r^T)\gamma_0^T(t_0,r^T)
\tag{A.4}
$$

Substitute Eq. (A.1), Eq. (A.3) into Eq. (7), which gives:

$$\frac{\pi^2 \sin\delta^A \left[\tau_0^A\left(t_0, r^A\right) \right]^2 \left(r^A\right)^2 h}{2\left|G^{*A}\right|} = \frac{\pi^2 \sin\delta^T \left[\tau_0^T\left(t_0, r^T\right) \right]^2 \left(r^T\right)^2 h}{2\left|G^{*T}\right|} \tag{A.5}$$

Combine Eq. (A.2), Eq. (A.3), Eq. (8) and Eq. (9), and give the following form:

$$\frac{DSE^A\left(t_0\right)}{RSE^A\left(t_0\right)} = \frac{DSE^T\left(t_0\right)}{RSE^T\left(t_0\right)} = \frac{2\pi\sin\delta^T}{\left(\sin\delta^T\left(\pi - 2\delta^T - \sin\left(2\delta^T\right)\right) - 2\cos^3\left(\delta^T\right)\right)} \tag{A.6}$$

Based on the torque balance Eq. (7), Eq. (14) and Eq. (15), the following expression can be obtained:

$$\frac{1}{2}\tau_0^A\left(t_0, r^A\right)\pi\left(r^A\right)^3 = \frac{1}{2}\tau_0^T\left(t_0, r^T\right)\pi\left(r^T\right)^3 \tag{A.7}$$

Combine Eq. (A.5), Eq. (A.6) with Eq. (A.7), the true radius r^T for the asphalt binder sample can be solved as below:

$$r^T = \left[\frac{\left|G^{*A}\right|}{\left|G^{*T}\right|}\right]^{1/4} r^A \tag{A.8}$$

Therefore, the damage density (Eq. (16)) can be obtained:

$$\phi = 1 - \frac{\pi\left(r^T\right)^2}{\pi\left(r^A\right)^2} = 1 - \sqrt{\frac{\left|G^{*A}\right|}{\left|G^{*T}\right|}} \tag{A.9}$$

Substitute Eqs. (A.8) into Eqs. (A.7), the following expression is given:

$$\frac{1}{2}\tau_0^A\left(t_0, r^A\right)\pi\left(r^A\right)^3 = \frac{1}{2}\tau_0^T\left(t_0, r^T\right)\pi\left[\frac{\left|G^{*A}\right|}{\left|G^{*T}\right|}\right]^{3/4}\left(r^A\right)^3 \tag{A.10}$$

Then, the true shear stress amplitude can be solved by:

$$\tau_0^T\left(t_0, r^T\right) = \left[\frac{\left|G^{*A}\right|}{\left|G^{*T}\right|}\right]^{4/3} \tau_0^A\left(t_0, r^A\right) \tag{A.11}$$

Finally, substitute Eq. (A.11) into Eq. (A.3), the true shear strain amplitude is determined by:

$$\gamma_0^T\left(t_0, r^T\right) = \left[\frac{\left|G^{*A}\right|}{\left|G^{*T}\right|}\right]^{6/11} \gamma_0^A\left(t_0, r^A\right) \tag{A.12}$$

Appendix B. Derivation of Eq. (21)

$DPSE_A(t)$ can be calculated as follows:

$$DPSE^A(t) = \iiint_{V^A} \left[\int_t^{t+2\pi/\omega} \tau^A(t,r) d\gamma_R^A(t,r) \right] dV \tag{B.1}$$

Based on Schapery's elastic–viscoelastic correspondence principle, the apparent pseudo shear strain $\gamma_R^A(t,r)$ can be defined as follows [43]:

$$\gamma_R^A(t,r) = \frac{\int_0^t G^A(t-\xi)\dfrac{d\gamma^A(\xi,r)}{d\xi}d\xi}{\left| G_R^{*A} \right|} \tag{B.2}$$

where $\gamma^A(\xi,r)$ is measured apparent shear strain at loading time ξ and at any position; ξ is a time variable of integration; $G^A(t-\xi)$ is apparent relaxation modulus at time $(t-\xi)$; $\left| G_R^{*A} \right|$ is reference modulus.

Substitute Eq. (1) into Eq. (B.2), which gives:

$$\gamma_R^A(t,r) = \frac{\int_0^t G^A(t-\xi)\dfrac{d\gamma_0^A(\xi,r)\sin(\omega\xi)}{d\xi}d\xi}{\left| G_R^{*A} \right|} = \frac{\int_0^t G^A(t-\xi)\gamma_0^A(\xi,r)\omega\cos(\omega\xi)d\xi}{\left| G_R^{*A} \right|} \tag{B.3}$$

in which $\gamma_0^A(\xi,r)$ is apparent shear strain amplitude at a given radius r and a given loading time ξ.

Let $\tau = t - \xi$, then, $\xi = t - \tau$, and when $\xi \in (0,t), \tau \in (t,0)$, Eq. (B.3) can be rearranged as below:

$$\gamma_R^A(t,r) = \frac{\omega\gamma_0^A(t-\tau,r)}{\left| G_R^{*A} \right|}\int_0^t G^A(\tau)\left[\cos(\omega t)\cos(\omega\tau) + \sin(\omega t)\sin(\omega\tau)\right]d\tau \tag{B.4}$$

According to the relationship between storage modulus $G^{A'}(\tau)$ and loss modulus $G^{A''}(\tau)$ of the shear complex modulus, give the following expression:

$$G^{A'}(\tau) = \omega\int_0^t G^A(\tau)\cos(\omega\tau)d\tau = G_{NLVE}^A\sin(\delta_{NLVE}^A) \tag{B.5}$$

35

$$G^{A''}(\tau) = \omega \int_0^t G^A(\tau)\sin(\omega\tau)d\tau = G_{NLVE}^A \cos\left(\delta_{NLVE}^A\right) \tag{B.6}$$

in which G_{NLVE}^A is apparent shear modulus at a nonlinear viscoelastic point; δ_{NLVE}^A is apparent phase angle at the nonlinear viscoelastic point.

Therefore, the pseudo shear strain $\gamma_R^A(t,r)$ can be expressed by:

$$
\begin{aligned}
\gamma_R^A(t,r) &= \frac{\gamma_0^A(t-\tau,r)}{\left|G_R^{*A}\right|} G_{NLVE}^A \left[\cos(\omega t)\sin\left(\delta_{NLVE}^A\right) + \sin(\omega t)\cos\left(\delta_{NLVE}^A\right)\right] \\
&= \frac{\gamma_0^A(t-\tau,r)}{\left|G_R^{*A}\right|} G_{NLVE}^A \sin\left(\omega t - \delta_{NLVE}^A\right)
\end{aligned}
\tag{B.7}
$$

When performing a strain-controlled rotational shear load, the apparent shear strain amplitude is constant. Therefore, $\gamma_0^A(t-\tau,r) = \gamma_0^A(t,r)$. If the apparent shear modulus G_{NLVE}^A at the nonlinear viscoelastic point as a reference modulus, $\gamma_R^A(t,r)$ will be expressed as below:

$$\gamma_R^A(t,r) = \gamma_0^A(t,r)\sin\left(\omega t - \delta_{NLVE}^A\right) \tag{B.8}$$

Then, substitute Eq. (B.8) into Eq. (B.1), the $DPSE^A(t)$ can be calculated as follows:

$$
\begin{aligned}
DPSE^A(t) &= \iiint_{V^A}\left[\int_t^{t+2\pi/\omega} \tau^A(t,r)d\gamma_R^A(t,r)\right]dV \\
&= \iiint_{V^A}\left[\int_t^{t+2\pi/\omega} \tau^A(t,r)d\left[\gamma_0^A(t,r)\sin\left(\omega t - \delta_{NLVE}^A\right)\right]\right]dV \\
&= \iiint_{V^A}\left[\int_t^{t+2\pi/\omega} \tau_0^A(t,r)\gamma_0^A(t,r)\sin\left(\omega t + \delta^A\right)\cos\left(\omega t - \delta_{NLVE}^A\right)d(\omega t)\right]dV \\
&= \iiint_{V^A}\left[\tau_0^A(t,r)\gamma_0^A(t,r)\int_t^{t+2\pi/\omega}\sin\left(\omega t + \delta^A\right)\cos\left(\omega t - \delta_{NLVE}^A\right)d(\omega t)\right]dV \\
&= \pi\sin\left(\delta^A - \delta_{NLVE}^A\right)\iiint_{V^A}\left[\tau_0^A(t,r)\gamma_0^A(t,r)\right]dV \\
&= \pi\sin\left(\delta^A - \delta_{NLVE}^A\right)\int_0^{2\pi}\int_o^{r^A}\int_0^h\left[\tau_0^A(t,r)\gamma_0^A(t,r)\right]rd\theta drdz \\
&= 2\pi^2\sin\left(\delta^A - \delta_{NLVE}^A\right)\tau_0\left(t_0,r^A\right)\gamma_0^A\left(t,r^A\right)\int_o^{r^A}\int_0^h\left(\frac{r}{r^A}\right)^2 rdrdz \\
&= \frac{1}{2}h\pi^2\left(r^A\right)^2 \tau_0\left(t_0,r^A\right)\gamma_0^A\left(t,r^A\right)\sin\left(\delta^A - \delta_{NLVE}^A\right)
\end{aligned}
\tag{B.9}
$$

where $\tau_0^A\left(t, r^A\right)$ is apparent shear stress at a given radius r^A and a given loading time t.

Combine Eq. (B.9), Eq. (18) and Eq. (19), the following equation can be obtained:

$$J_R = \frac{\dfrac{1}{2}h\pi^2\left(r^A\right)^2\tau_0\left(t_0, r^A\right)\gamma_0^A\left(t, r^A\right)\sin\left(\delta^A - \delta_{NLVE}^A\right)}{\pi\left(r^A\right)^2 \partial\phi/\partial t} \tag{B.10}$$

Then, substitute Eq. (B.10) into Eq. (17), and gives the following equation:

$$\frac{d\phi}{dt} = A\left(\frac{\dfrac{1}{2}h\pi^2\left(r^A\right)^2\tau_0\left(t_0, r^A\right)\gamma_0^A\left(t, r^A\right)\sin\left(\delta^A - \delta_{NLVE}^A\right)}{\pi\left(r^A\right)^2 \partial\phi/\partial t}\right)^n \tag{B.11}$$

Finally, substitute Eq. (3) into Eq. (B.11), the Eq. (21) can be obtained:

$$\frac{d\phi}{dt} = A^{1/(n+1)}\left[\frac{1}{2}\pi h\left|G^{*A}\right|\left[\gamma_0^A\left(t, r^A\right)\right]^2\sin\left(\delta^A - \delta_{NLVE}^A\right)\right]^{n/(n+1)} \tag{B.12}$$

References

[1] Hicks, R. G., Finn, F. N., Monismith, C. L., & Leahy, R. B. (1993). Validation of SHRP binder specification through mix testing (with discussion). *Journal of the Association of Asphalt Paving Technologists*, *62*.

[2] Kim, Y. R., Lee, H. J., & Little, D. N. (1997). Fatigue characterization of asphalt concrete using viscoelasticity and continuum damage theory (with discussion). *Journal of the Association of Asphalt Paving Technologists*, *66*.

[3] Reese, R. (1997). Properties of aged asphalt binder related to asphalt concrete fatigue life. *Journal of the Association of Asphalt Paving Technologists*, *66*.

[4] Anderson, D. A., & Kennedy, T. W. (1993). Development of SHRP binder specification (with discussion). *Journal of the Association of Asphalt Paving Technologists*, *62*.

[5] Ghuzlan, K. A., & Carpenter, S. H. (2000). Energy-derived, damage-based failure criterion for fatigue testing. *Transportation research record*, 1723(1), 141-149.

[6] Bonnetti, K. S., Nam, K., & Bahia, H. U. (2002). Measuring and defining fatigue behavior of asphalt binders. *Transportation Research Record*, *1810*(1), 33-43.

[7] Wang, C., Zhang, H., Castorena, C., Zhang, J., & Kim, Y. R. (2016). Identifying fatigue failure in asphalt binder time sweep tests. *Construction and Building Materials*, 121(SEP.15), 535-546.

[8] Shen, S., Airey, G. D., Carpenter, S. H., & Huang, H. (2006). A dissipated energy approach to fatigue evaluation. *Road materials and pavement design*, *7*(1), 47-69.

[9] Shen, S., & Lu, X. (2011). Energy based laboratory fatigue failure criteria for asphalt materials. *Journal of Testing and Evaluation*, *39*(3), 313-320.

[10] Subhy, A., Presti, D. L., & Airey, G. (2017). New simplified approach for obtaining a reliable plateau value in fatigue analysis of bituminous materials. *Engineering Failure Analysis*, *79*, 263-273.

[11] Hintz, C., & Bahia, H. (2013). Understanding mechanisms leading to asphalt binder fatigue in the dynamic shear rheometer. *Road Materials and Pavement Design*, *14*(sup2), 231-251.

[12] Shan, L., Tian, S., He, H., & Ren, N. (2017). Internal crack growth of asphalt binders during shear fatigue process. *Fuel*, *189*, 293-300.

[13] Zhang, Y., & Gao, Y. (2019). Predicting crack growth in viscoelastic bitumen under a rotational shear fatigue load. *Road Materials and Pavement Design*, 1-20.

[14] Li, L., Gao, Y., & Zhang, Y. (2020). Crack length based healing characterisation of bitumen at different levels of cracking damage. *Journal of Cleaner Production*, *258*, 120709.

[15] Sankararaman, S., Ling, Y., & Mahadevan, S. (2011). Uncertainty quantification and model validation of fatigue crack growth prediction. *Engineering Fracture Mechanics*, *78*(7), 1487-1504.

[16] Tryon, R. G., & Cruse, T. A. (1998). A reliability-based model to predict scatter in fatigue crack nucleation life. *Fatigue & Fracture of Engineering Materials & Structures*, *21*(3), 257-267.

[17] Wills, J., Caro, S., & Braham, A. (2019). Influence of material heterogeneity in the fracture of asphalt mixtures, *International Journal of Pavement Engineering*, 20:7, 747-760.

[18] Singh, P., & Swamy, A. K. (2019). Probabilistic characterisation of damage characteristic curve of asphalt concrete mixtures. *International Journal of Pavement Engineering*, 20:6, 659-668.

[19] Bogdanoff, J. L., & Kozin, F. (1985). Probabilistic models of cumulative damage (Book). *New York, Wiley-Interscience, 1985, 350 p.*

[20] Kozin, F., & Bogdanoff, J. L. (1981). A critical analysis of some probabilistic models of fatigue crack growth. *Engineering Fracture Mechanics*, *14*(1), 59-89.

[21] Kozin, F., & Bogdanoff, J. L. (1989). Probabilistic models of fatigue crack growth: results and speculations. *Nuclear Engineering & Design, 115*(1), 143-171.

[22] Yang, J. N., & Manning, S. D. (1990). Stochastic crack growth analysis methodologies for metallic structures. *Engineering Fracture Mechanics, 37*(5), 1105-1124.

[23] Wu, W. F., & Ni, C. C. (2003). A study of stochastic fatigue crack growth modeling through experimental data. *Probabilistic Engineering Mechanics*, *18*(2), 107-118.

[24] Casciati, F., Colombi, P., & Faravelli, L. (2007). Inherent variability of an experimental crack growth curve. *Structural safety*, *29*(1), 66-76.

[25] Chiquet, J., Limnios, N., & Eid, M. (2009). Piecewise deterministic Markov processes applied to fatigue crack growth modelling. *Journal of Statistical Planning and Inference*, *139*(5), 1657-1667.

[26] Guida, M., & Penta, F. (2015). A gamma process model for the analysis of fatigue crack growth data. *Engineering Fracture Mechanics*, *142*, 21-49.

[27] Sadek, H., Masad, E., Al-Khalid, H., & Sirin, O. (2016). Probabilistic analysis of fatigue life for asphalt mixtures using the viscoelastic continuum damage approach. *Construction and Building Materials*, *126*, 227-244.

[28] Sadek, H., Sadeq, M., Masad, E., Al-Khalid, H., & Sirin, O. (2019). Probabilistic Viscoelastic Continuum Damage Analysis of Fatigue Life of Warm-Mix Asphalt. *Journal of Transportation Engineering, Part B: Pavements*, *145*(3), 04019024.

[29] Kassem, H., Chehab, G., & Najjar, S. (2019). Development of probabilistic viscoelastic continuum damage model for asphalt concrete. *Transportation Research Record*, *2673*(5), 285-298.

[30] China, M. (2011). Standard Test Methods of Bitumen and Bituminous Mixtures for Highway Engineering: JTG E20-2011.

[31] Luo, X., R. Luo, and R.L. Lytton (2013a). Characterization of Fatigue Damage in Asphalt Mixtures Using Pseudo Strain Energy. *Journal of Materials in Civil Engineering*, 25(2), 208-218.

[32] Luo, X., Luo, R., & Lytton, R. L. (2014a). Energy-based mechanistic approach for damage characterization of pre-flawed visco-elasto-plastic materials. *Mechanics of Materials, 70*, 18-32.

[33] Luo, X., Luo, R., & Lytton, R. L. (2014b). Energy-based crack initiation criterion for viscoelastoplastic materials with distributed cracks. *Journal of Engineering Mechanics, 141*(2), 04014114.

[34] Luo, X., Birgisson, B., & Lytton, R. L. (2020). Kinetics of healing of asphalt mixtures. *Journal of Cleaner Production*, *252*, 119790.

[35] Luo, X., Li, H., Deng, Y., & Zhang, Y. (2020). Energy-Based Kinetics Approach for Coupled Viscoplasticity and Viscofracture of Asphalt Mixtures. *Journal of Engineering Mechanics*, 146(9), 04020100.

[36] Li, H., Luo, X., Yan, W., & Zhang, Y. (2020). Energy-Based Mechanistic Approach for Crack Growth Characterization of Asphalt Binder. *Mechanics of Materials*, 103462.

[37] Li, H., Luo, X., Yan, W., & Zhang, Y. (2020). Pseudo Energy-based Kinetic Characterization of Fatigue in Asphalt Binders. *China Journal of Highway and Transport*, 2020, 33(10): 115-124.

[38] Luo, X., Zhang, Y., & Lytton, R. L. (2016). Implementation of pseudo J-integral based Paris' law for fatigue cracking in asphalt mixtures and pavements. *Materials and Structures*, 49(9), 3713-3732.

[39] Luo, X., Luo, R., & Lytton, R. L. (2013c). Modified Paris's law to predict entire crack growth in asphalt mixtures. *Transportation research record*, *2373*(1), 54-62.

[40] Jirandehi, A. P., & Khonsari, M. M. (2020). Microstructure-Sensitive estimation of fatigue life using cyclic thermodynamic entropy as an index for metals. *Theoretical and Applied Fracture Mechanics*, 102854.

[41] Jirandehi, A. P., & Khonsari, M. M. (2020). On the determination of cyclic plastic strain energy with the provision for microplasticity. *International Journal of Fatigue*, 142, 105966.

[42] Yang, J. N., Manning, S. D., Hsi, W. H., & Rudd, J. L. (1987). Stochastic crack growth models for applications to aircraft structures. In *Probabilistic fracture mechanics and reliability* (pp. 171-211). Springer, Dordrecht.

[43] Schapery, R. A. (1984). Correspondence principles and a generalized J integral for large deformation and fracture analysis of viscoelastic media. *International Journal of Fracture*, *25*(3), 195-223.

Conflict of Interest

The authors declare that they have no conflict of interest.

[44]